LETTER

Direct observation of electron propagation and dielectric screening on the atomic length scale

S. Neppl[1,2]†, R. Ernstorfer[3], A. L. Cavalieri[4,5,6], C. Lemell[7], G. Wachter[7], E. Magerl[2], E. M. Bothschafter[8], M. Jobst[1,2], M. Hofstetter[2,8], U. Kleineberg[2,8], J. V. Barth[1], D. Menzel[1,3], J. Burgdörfer[7,9], P. Feulner[1], F. Krausz[2,8] & R. Kienberger[1,2]

The propagation and transport of electrons in crystals is a fundamental process pertaining to the functioning of most electronic devices. Microscopic theories describe this phenomenon as being based on the motion of Bloch wave packets[1]. These wave packets are superpositions of individual Bloch states with the group velocity determined by the dispersion of the electronic band structure near the central wavevector in momentum space[1]. This concept has been verified experimentally in artificial superlattices by the observation of Bloch oscillations[2]—periodic oscillations of electrons in real and momentum space. Here we present a direct observation of electron wave packet motion in a real-space and real-time experiment, on length and time scales shorter than the Bloch oscillation amplitude and period. We show that attosecond metrology[3] (1 as = 10^{-18} seconds) now enables quantitative insight into weakly disturbed electron wave packet propagation on the atomic length scale without being hampered by scattering effects, which inevitably occur over macroscopic propagation length scales. We use sub-femtosecond (less than 10^{-15} seconds) extreme-ultraviolet light pulses[3] to launch photoelectron wave packets inside a tungsten crystal that is covered by magnesium films of varied, well-defined thicknesses of a few ångströms[4]. Probing the moment of arrival of the wave packets at the surface with attosecond precision reveals free-electron-like, ballistic propagation behaviour inside the magnesium adlayer—constituting the semi-classical limit of Bloch wave packet motion. Real-time access to electron transport through atomic layers and interfaces promises unprecedented insight into phenomena that may enable the scaling of electronic and photonic circuits to atomic dimensions. In addition, this experiment allows us to determine the penetration depth of electrical fields at optical frequencies at solid interfaces on the atomic scale.

A detailed microscopic understanding and control of electronic and optical properties of solids depends on our ability to access the dynamics of electrons on atomic time and length scales. Tracking the propagation of electrons in real time requires the ability to pinpoint their position at a rate comparable to the time on which interactions with other electrons and the crystal lattice may affect their trajectories inside the material. In a classical picture, the upper bound for the necessary temporal resolution is therefore the time it takes the electrons to travel the several-ångström distance between neighbouring atoms. This implies transit times well below one femtosecond even for kinetic energies as low as $E_{kin} \approx 1$ eV. Previous time-resolving studies on electron propagation in condensed matter employed laser-based spectroscopic techniques to reveal ballistic currents and drift motion of charge carriers[5–8]. Restricted to the pico- and femtosecond timescales, they are able to probe carrier dynamics averaged over several hundreds of nanometres. In contrast, the experimental approach demonstrated here offers quantitative real-time access to electron transport on the inter-atomic length scale.

Figure 1 illustrates the basic principle of the experiment. Attosecond extreme-ultraviolet (XUV) light pulses generate Bloch electron wave packets with final-state energies substantially above the vacuum level. Electron wave packets with a sufficiently large momentum component along the surface-normal direction z contribute to the photoelectron current reaching the time-of-flight detector. Conventional photoelectron spectroscopy is restricted to measuring the energy and momentum distributions of photoelectrons. Here we additionally capture the temporal profile of the photoemission process by having the ejected electrons interact with the controlled few-cycle electric field of a visible/near-infrared (henceforth referred to as 'NIR') laser pulse covering the 500–1,000 nm spectral range and synchronized, with attosecond precision, to the XUV pulse.

As this field modifies ('streaks') the momentum of a photoelectron in proportion to the laser vector potential $A_L(z, t)$ at the instant t the electron enters the NIR field[3,9,10], the temporal profile of the electron wave packet leaving the sample is mapped onto its final momentum distribution. Full streaking spectrograms obtained by recording these laser-modulated electron energy distributions as a function of delay Δt between the XUV and the NIR pulses are therefore highly sensitive to the spatio-temporal characteristics of both the photoelectron wave packet and the streaking laser field on the ångström length scale and the attosecond timescale[9–11].

Direct (time-domain) access to these electronic and optical wave packets promises a unique insight into the photoelectric effect, including underlying electron propagation and phenomena as fundamental as dielectric screening of light fields at solid surfaces. Here we show that this can be achieved by combining state-of-the-art attosecond timing metrology (chronoscopy)[3,9–11] with sample engineering on the ångström level[4,12].

When excited from Bloch states inside the crystal to positive-energy states[13], photoelectrons are not immediately exposed to the streaking field because the electric field amplitude is substantially reduced (or screened) at the topmost layer by the response of the metal electrons. Therefore, the time delay associated with the propagation of the respective Bloch wave packets towards the surface (included in both the quantum-mechanical one-step[13] and the semi-classical three-step[14,15] description of photoemission) is encoded in the streaking spectrogram[9–11]. Differences in the propagation times of electrons ejected from different initial states manifest themselves as a temporal offset between the respective streaking traces[9–11] (see Fig. 1a). Previous studies on single crystals revealed a considerable time delay between the emission of core-level and conduction band (CB) photoelectrons from the transition metal tungsten W(110)[9], whereas such a delay was found to be absent

[1]Physik-Department, Technische Universität München, 85747 Garching, Germany. [2]Max-Planck-Institut für Quantenoptik, Hans-Kopfermann-Straße 1, 85748 Garching, Germany. [3]Fritz-Haber-Institut der Max-Planck-Gesellschaft, Faradayweg 4–6, 14195 Berlin, Germany. [4]Max Planck Institute for the Structure and Dynamics of Matter, Luruper Chaussee 149, 22761 Hamburg, Germany. [5]Fakultät für Mathematik, Informatik und Naturwissenschaften, University of Hamburg, Luruper Chaussee 149, 22761 Hamburg, Germany. [6]Center for Free-Electron Laser Science (CFEL), Luruper Chaussee 149, 22761 Hamburg, Germany. [7]Institute for Theoretical Physics, Vienna University of Technology, Wiedner Hauptstrasse 8-10/E136, A-1040 Vienna, Austria. [8]Fakultät für Physik, Ludwig-Maximilians-Universität München, Am Coulombwall 1, D-85748 Garching, Germany. [9]Institute of Nuclear Research of the Hungarian Academy of Sciences (ATOMKI), 4001 Debrecen, Hungary. †Present address: Lawrence Berkeley National Laboratory, Chemical Sciences Division, Berkeley, California 94720, USA.

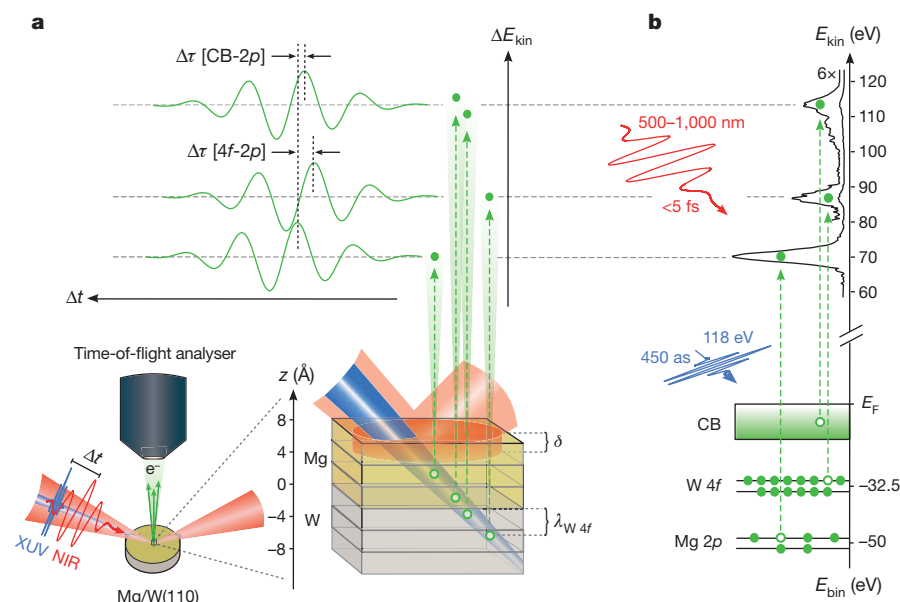**Figure 1 | Spatio-temporal dynamics in attosecond photoemission from Mg/W(110). a**, Principle of the experiment: photoelectrons (green dots) are launched inside a tungsten W(110) crystal and a magnesium (Mg) overlayer a few ångströms thick by an XUV pulse of ~450 as, and are detected in ultrahigh vacuum with a time-of-flight analyser. At the surface, the arrival times of electrons released from different initial states are probed by streaking their associated electron energy distributions with a 2×10^{11} W cm^{-2} strong electric field delivered by a sub-5 fs broadband linearly polarized visible/near-infrared laser pulse. Relative time delays $\Delta\tau$ developing during the propagation of the photoelectrons to the metal–vacuum interface are detected as temporal shifts between their streaked energy distributions. The time shifts $\Delta\tau$ are

sensitive to the atomic-scale electron transport characteristics (quantified by the inelastic mean free path λ; indicated only for the W $4f$ electrons), the Mg overlayer thickness and the screening behaviour of the laser field at the solid–vacuum interface. **b**, Schematic energy-level diagram for the probed electronic transitions. The central XUV photon energy of ~118 eV allows the simultaneous excitation of Mg $2p$, W $4f$ and the joint CB states (binding energy E_{bin} as indicated). A background-corrected photoelectron spectrum of $n = 4$ adlayers of Mg on W(110) in the absence of the laser field is shown as the black solid line. For better visibility, the strength of the CB and W $4f$ signals are magnified by a factor of six.
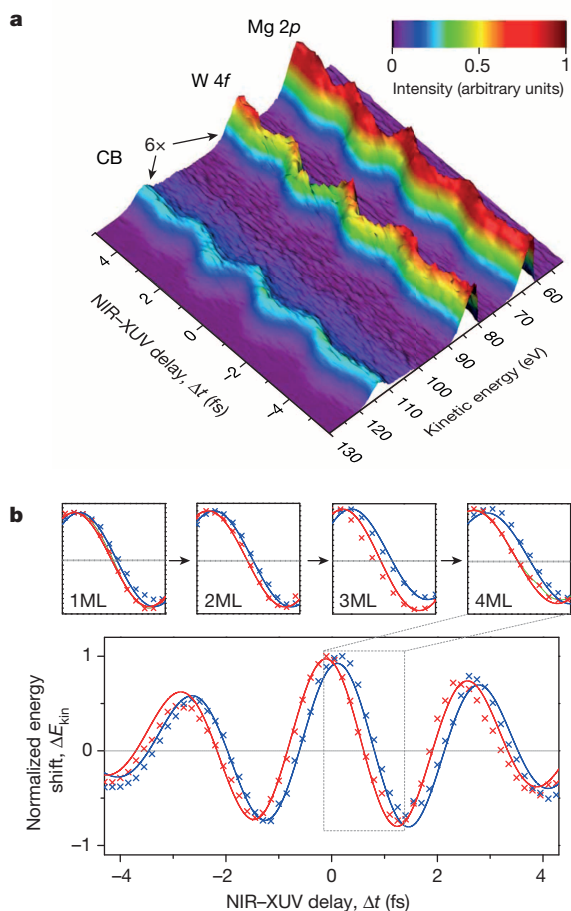
in the photoemission from the free-electron metal magnesium Mg(0001)[10]. Theoretical models have addressed different contributions such as may arise from the band structure of the material[9,16,17], the spatial characteristics of the initial-state wavefunctions[18–21], and elastic and inelastic scattering effects[9,22]. These models also differ from each other in the way that the screening of the laser field at the surface is taken into account when calculating the photoemission time delays[19,22,23]. To isolate the atomic-scale electron propagation process from this multitude of disparate effects, we investigate hybrid metallic samples consisting of a controllable number n of Mg adlayers on a W(110) crystal[12,24] (see Fig. 1a and Supplementary Information for details) and contrast the measured time shifts with electron transport calculations.

In our experiments, XUV pulses with a duration of about 450 as and a photon energy of $\hbar\omega_{XUV} = 118$ eV simultaneously generate photoelectrons from core states of the substrate (W $4f$) and adlayer (Mg $2p$), as well as from the energetically overlapping CB states of both materials (Fig. 1b). A representative streaking spectrogram for $n = 4$ Mg adlayers on W(110) is shown in Fig. 2a. Despite the ~80% attenuation of the W

Figure 2 | Attosecond time-resolved photoemission from Mg/W(110). a, Representative streaking spectrogram for $n = 4$ Mg monolayers (ML). All photoelectron spectra are corrected for the inelastic electron background signal. The strength of the CB and W $4f$ signals is magnified by a factor of 6 for better visibility. **b**, Exemplary timing analysis of the Mg $2p$ and W $4f$ core-level electrons: the first moments calculated from their respective kinetic energy distributions are shown as red crosses (Mg $2p$) and blue crosses (W $4f$) as functions of NIR–XUV delay Δt. A global fit of the resultant streaking traces to a parameterized waveform for the NIR vector potential (solid lines) reveals a relative time shift $\Delta\tau[4f - 2p]$, which can be identified with the time delay occurring during the release of the electrons from the metal surface. Insets illustrate the evolution of $\Delta\tau[4f - 2p]$ for $0 < n \le 4$. Regions exhibiting the largest gradient of the streaking field (corresponding to the highest temporal resolution) are highlighted. An analogous evaluation of $\Delta\tau[CB - 2p]$ is presented in the Supplementary Information.

substrate photoemission due to inelastic scattering in the Mg overlayer, the streaked W 4*f* and CB photoemission lines are clearly discernible. They are also sufficiently separated from each other and from the Mg 2*p* line over the entire range of XUV–NIR delays, Δ*t*, to guarantee an accurate quantitative analysis of their relative emission dynamics[9–11]. In what follows, we reference the emission times of the W 4*f* and CB electrons to the Mg 2*p* emission from the Mg overlayer and denote the resultant relative delays as Δτ[4*f* - 2*p*] and Δτ[CB - 2*p*], respectively.

We begin with an analysis of Δτ[4*f* - 2*p*] because the involved photoelectrons originate from atomic-like states that are entirely localized in the W(110) substrate or the Mg overlayer. This allows unambiguous interrelation of the measured time shifts and the well-defined propagation distances in the Mg adlayer systems, which may not perfectly apply to CB electrons owing to the delocalized character of the CB initial-state

wavefunctions[19–21]. Relative time shifts Δτ[4*f* -2*p*] extracted with a robust quantum-mechanical fitting scheme[9–11] (see Supplementary Information) from streaking spectrograms at different Mg coverages are summarized in Fig. 3a (blue diamonds). They reveal a distinct monotonic increase of Δτ[4*f* - 2*p*] with the number *n* of Mg adlayers, reaching Δτ[4*f* - 2*p*] = 215 ± 20 as for a Mg film 10.4 Å (*n* = 4) thick. We verified this trend using a simpler analysis that compares the first moments of the streaked W 4*f* and Mg 2*p* energy distributions as functions of Δ*t* (Fig. 2b; see Supplementary Information).

The simplest description of the electron propagation is to consider ballistic motion of the centroid of a Bloch wave packet as a free point-like electron in one dimension[25]. For the Mg layers, Δτ[4*f* - 2*p*] is then dominated by the average propagation time τ_{4f} of the 4*f*-derived wave packets with central wavevectors $k = k_0$ travelling at a group velocity $v_{4f} = \dfrac{\mathrm{d}E(k)}{\hbar \mathrm{d}k}|_{k=k_0}$. Owing to the free-electron-like band-structure of Mg[10,26], we can assume that $v_{4f} \approx \sqrt{2E_{\mathrm{kin}}/m_e}$, where m_e is the free electron mass. The kinetic energy of the photoelectrons inside the Mg layer amounts to $E_{\mathrm{kin}} \approx 93$ eV (the photon energy is $\hbar\omega_{\mathrm{XUV}} = 118$ eV, the binding energy of the 4*f* electrons is $E_b \approx 32.5$ eV, the Fermi energy of bulk Mg is $E_{\mathrm{Fermi}} \approx 7$ eV), leading to an average group velocity of $v_{4f} \approx 0.057$ Å as^{-1}. We therefore expect τ_{4f}—which is the upper limit for Δτ[4*f* - 2*p*]—to increase almost linearly with the number of Mg adlayers *n*, according to $\tau_{4f} \approx n \times d/v_{4f} \approx n \times 45$ as, where $d = 2.6$ Å is the interlayer spacing of the epitaxial Mg films[12]. A linear fit to the experimental data of Fig. 3a yields a delay of ~42 as per adlayer. The good agreement between experiment and model prediction provides conclusive evidence for the atomic-scale ballistic propagation of the 4*f* electrons being the microscopic origin of the observed time shifts in the spectrograms and also corroborates free-electron-like transport in Mg.

This interpretation is substantiated by electron transport simulations[22] of the ballistic motion of the W 4*f*, Mg 2*p* and CB electrons in the Mg/W(110) systems. In general, time delays obtained from such transport calculations are sensitive to (1) the average group velocities of the electrons at the relevant energies, (2) their energy-dependent inelastic mean free path $\lambda(E_{\mathrm{kin}})$ in the traversed materials and (3) the spatio-temporal profile of the streaking field near the surface[22]. The average group velocities can be deduced from electronic structure calculations[9,17] and all relevant values of $\lambda(E_{\mathrm{kin}})$ are known from synchrotron experiments[10]
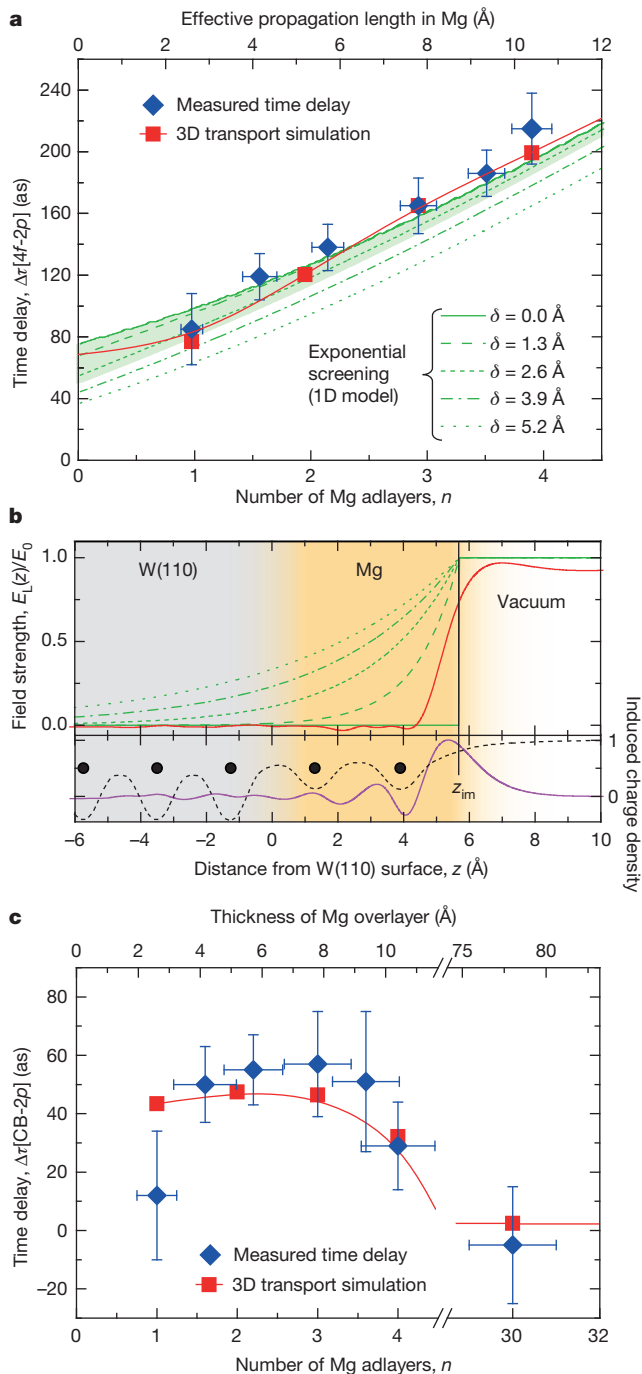

a

b

c

Figure 3 | **Atomic-scale photoelectron transport and screening of the incident light field. a**, Time delays Δτ[4*f* - 2*p*] between the release of W 4*f* and Mg 2*p* electrons extracted from a large set of streaking spectrograms with different numbers of Mg adlayers are shown as blue diamonds. Error bars denote full standard deviations and are obtained by averaging measurements performed under similar experimental conditions. Fractional adlayers correspond to dispersed two-dimensional islands (on top of a completed Mg layer) that coalesce upon further Mg deposition. Green lines are time delays predicted by our one-dimensional (1D) simulation of the photoelectron release dynamics for different screening lengths δ assuming an exponentially decaying normal component of the incident NIR streaking field at the metal–vacuum interface according to $E_L(z, t) = E_0 e^{-(z-z_{\mathrm{im}})/\delta}$. The light-green-shaded area highlights the screening scenarios compatible with the experiment. Red squares indicate time delays derived from a full three-dimensional electron transport model (the red line is a guide to the eye). **b**, The upper panel illustrates the different screening scenarios for $E_L(z, t)$ considered in **a** for the example of *n* = 2 Mg adlayers (orange shading) on W(110) (grey shading). The red line is the spatial variation of $E_L(z, t)$ at the interface predicted by TDDFT. The lower panel is a snapshot of the NIR-induced charge density at the metal–vacuum interface at the maximum of the laser pulse derived by TDDFT (magenta line). The position of the dynamic image plane z_{im} is indicated as a vertical black solid line. The lattice potential (averaged parallel to the crystal surface) employed in the DFT calculations is shown as a dotted black line. The positions of the Mg and W atoms at the interface along the surface normal are indicated as black dots. The gradual transitions from the W electronic structure (grey) to the Mg electronic structure (orange) and to the vacuum (white) are indicated in the background colours. **c**, Comparison of time shifts Δτ[CB - 2*p*] measured between the emission of CB and Mg 2*p* electrons with time delays predicted by the three-dimensional (3D) electron transport model.

or theory[27]. As a consequence, our experiments open up the opportunity to explore the spatial variation of the laser field's $E_L(z)$ component normal to the surface (z axis) on the ångström length scale.

Screening at metallic surfaces becomes effective near the so-called image plane z_{im}, located about a half-layer spacing outside the centre of the topmost atomic layer[28,29]. As our method probes the optical near-field at the metal–vacuum interface, the commonly used Fresnel equations based on macroscopic properties of target components with perfectly sharp interfaces cannot be applied. Instead, a phenomenological exponential decay $E_L(z, t) = E_0 e^{-(z-z_{im})/\delta}$ of the surface-normal component of the field inside the material appears to be a reasonable assumption[18,23]. We therefore modelled the impact of different screening lengths δ, that is, the length scale on which the stepwise prediction of the Fresnel formula does not apply, on the time delays $\Delta\tau[4f\text{-}2p]$ using one-dimensional electron transport simulations (see Supplementary Information). The time delays $\Delta\tau[4f\text{-}2p]$ predicted by this simple model as a function of n and δ are plotted as green lines in Fig. 3a. Apparently, only the range $0 \leq \delta \leq 3$ Å is compatible with the experiment and the associated error bars, indicating a screening within one atomic layer of Mg.

To scrutinize the origin of this rapid interfacial screening, we used time-dependent density functional theory (TDDFT)[30] to calculate $E_L(z,t)$ for the Mg/W(110) systems. The surface-normal component of the incident laser field induces a polarization charge layer at the metal surface that shields the interior of the solid against the external electric field. The centroid of the induced screening charge density defines the exact position z_{im} of the image plane, which marks the microscopic onset of the local screening process[30] (see Fig. 3b). Both the positions $z_{im, n}$ and the width δ_n of the induced screening charge are found to be almost independent of the number n of Mg layers. The key finding is that the laser field is already fully screened at the plane defined by the centre of the atoms of the topmost layer for all Mg/W(110) systems, in agreement with the conclusion drawn from the comparison of our experimental data with the phenomenological modelling.

Finally, we incorporated the abrupt screening of the streaking field at the surface revealed by TDDFT in a full three-dimensional streaking simulation[22] of the electron propagation in Mg/W(110) (see Supplementary Information for a detailed description). Similar to the above-mentioned one-dimensional model, wave packet propagation is simulated by the transport of an ensemble of point-like charges taking stochastic inelastic and elastic scattering events into account. The time delays $\Delta\tau[4f\text{-}2p]$ predicted by these calculations (red squares in Fig. 3a) are in good agreement with the experiment.

Compared to the core-level photoemission time delay $\Delta\tau[W\,4f\text{-}2p]$, the temporal shift of the conduction band emission $\Delta\tau[CB\text{-}2p]$ (Fig. 3c) is distinctly smaller and exhibits a strikingly different dependence on the number of Mg adlayers. A detailed analysis of $\Delta\tau[CB\text{-}2p]$ within electron transport models is complicated by different (spectrally unresolved) contributions of W(110)- and Mg-derived states to the joint CB feature at $E_{kin} \approx 115$ eV. However, by weighting the excitation probabilities from these different initial states according to their atomic photoexcitation cross-sections (see Supplementary Information), we achieved good overall agreement with the experimental results, and correctly reproduced the vanishing $\Delta\tau[CB\text{-}2p]$ time delay for bulk Mg[10]. This suggests that our approximate treatment of the Bloch wave packet propagation and the dielectric screening response remains valid also for more delocalized initial electronic states, in contrast to recent predictions[23,24].

We emphasize that $\Delta\tau[CB\text{-}2p]$ for $n = 1$ is overestimated in our transport model and lies outside the experimental error margin. A deviation from the present model appears likely for the Mg/W(110) monolayer system, since strong mixing of band states at the interface may lead to a deviation of the initial-state band structure and excitation cross-sections from their bulk characteristics[24]. A detailed discussion of this phenomenon is beyond the scope of the present study, but indicates the potential of attosecond photoelectron spectroscopy to probe interfacial hybridization between electronic states directly in the time domain. Therefore this technique may be applied to phenomena not describable by a

simple combination of separate electronic structure models for bulk and surface layers.

This work extends the realm of attosecond spectroscopy to the direct observation of atomic-scale propagation and damping of electronic and optical wave packets at solid surfaces. The resultant insight into attosecond temporal and—simultaneously—ångström spatial dimensions opens the door for understanding and exploring electron transport phenomena on the atomic scale and the dielectric response of solids at optical frequencies. Applied to overlayer materials with non-free-electron-like positive-energy states, such studies will shed light on whether stationary band structure can be used to predict atomic-scale electron propagation on ultrashort timescales. Extrapolation of coverage-dependent streaking spectroscopy to the sub-monolayer regime will provide access to absolute photoemission times and possible intrinsic (atomic) retardation effects in the photoemission process. Beyond addressing these fundamental questions, attosecond electron transport chronoscopy may prove instrumental in advancing electronic and photonic circuits towards atomic dimensions.

1. Bloch, F. Über die Quantenmechanik der Elektronen in Kristallgittern. *Z. Phys.* **52,** 555–600 (1929).
2. Leo, K., Bolivar, P. H., Brüggemann, F., Schwedler, R. & Köhler, K. Observation of Bloch oscillations in a semiconductor superlattice. *Solid State Commun.* **84,** 943–946 (1992).
3. Hentschel, M. *et al.* Attosecond metrology. *Nature* **414,** 509–513 (2001).
4. Schiller, F., Heber, M., Servedio, V. D. P. & Laubschat, C. Electronic structure of Mg: from monolayers to bulk. *Phys. Rev. B* **70,** 125106 (2004).
5. Gremillet, L. *et al.* Time-resolved observation of ultrahigh intensity laser-produced electron jets propagating through transparent solid targets. *Phys. Rev. Lett.* **83,** 5015–5018 (1999).
6. Sha, W., Norris, T. B., Schaff, W. J. & Meyer, K. E. Time-resolved ballistic acceleration of electrons in a GaAs quantum-well structure. *Phys. Rev. Lett.* **67,** 2553–2556 (1991).
7. Sha, W., Rhee, J.-k., Member, S., Norris, T. B. & Schaff, W. J. Transient carrier and field dynamics in quantum- well parallel transport: from the ballistic to the quasi-equilibrium regime. *IEEE J. Quantum Electron.* **28,** 2445–2455 (1992).
8. Shaner, E. & Lyon, S. Picosecond time-resolved two-dimensional ballistic electron transport. *Phys. Rev. Lett.* **93,** 037402 (2004).
9. Cavalieri, A. L. *et al.* Attosecond spectroscopy in condensed matter. *Nature* **449,** 1029–1032 (2007).
10. Neppl, S. *et al.* Attosecond time-resolved photoemission from core and valence states of magnesium. *Phys. Rev. Lett.* **109,** 22–26 (2012).
11. Schultze, M. *et al.* Delay in photoemission. *Science* **328,** 1658–1662 (2010).
12. Aballe, L., Barinov, A., Locatelli, A., Mentes, T. O. & Kiskinova, M. Initial stages of heteroepitaxial Mg growth on W(110): early condensation, anisotropic strain, and self-organized patterns. *Phys. Rev. B* **75,** 115411 (2007).
13. Mahan, G. D. Theory of photoemission in simple metals. *Phys. Rev. B* **2,** 4334–4350 (1970).
14. Berglund, C. N. & Spicer, W. E. Photoemission studies of copper and silver: theory. *Phys. Rev.* **136,** A1030–A1044 (1964).
15. Feibelman, P. J. & Eastman, D. E. Photoemission spectroscopy—correspondence between quantum theory and experimental phenomenology. *Phys. Rev. B* **10,** 4932–4947 (1974).
16. Borisov, G., Sánchez-Portal, D., Kazansky, K. & Echenique, P. M. Resonant and nonresonant processes in attosecond streaking from metals. *Phys. Rev. B* **87,** 121110 (2013).
17. Krasovskii, E. E. Attosecond spectroscopy of solids: streaking phase shift due to lattice scattering. *Phys. Rev. B* **84,** 195106 (2011).
18. Liao, Q. & Thumm, U. Attosecond time-resolved photoelectron dispersion and photoemission time delays. *Phys. Rev. Lett.* **112,** 023602 (2014).
19. Kazansky, A. K. & Echenique, P. M. One-electron model for the electronic response of metal surfaces to subfemtosecond photoexcitation. *Phys. Rev. Lett.* **102,** 177401 (2009).
20. Zhang, C. H. & Thumm, U. Attosecond photoelectron spectroscopy of metal surfaces. *Phys. Rev. Lett.* **102,** 123601 (2009).
21. Zhang, C. H. & Thumm, U. Effect of wave-function localization on the time delay in photoemission from surfaces. *Phys. Rev. A* **84,** 033401 (2011).
22. Lemell, C., Solleder, B., Tökési, K. & Burgdörfer, J. Simulation of attosecond streaking of electrons emitted from a tungsten surface. *Phys. Rev. A* **79,** 62901 (2009).
23. Zhang, C. H. & Thumm, U. Probing dielectric-response effects with attosecond time-resolved streaked photoelectron spectroscopy of metal surfaces. *Phys. Rev. B* **84,** 1–7 (2011).
24. Vinogradov, N., Marchenko, D., Shikin, A., Adamchuk, V. & Rader, O. Size effects in ultrathin Mg/W(110) films: quantum electronic states. *Phys. Solid State* **51,** 179–188 (2009).
25. Kroemer, H. On the group velocity of Bloch waves. *Proc. IEEE* **63,** 988 (1975).

26. Bartynski, R. A., Gaylord, R. H., Gustafsson, T. & Plummer, E. W. Angle-resolved photoemission study of the surface and bulk electronic structure of Mg(0001) and Mg(112-bar0). *Phys. Rev. B* **33,** 3644–3665 (1986).
27. Tanuma, S., Powell, C. J. & Penn, D. R. Calculations of electron inelastic mean free paths. IX. Data for 41 elemental solids over the 50 eV to 30 keV range. *Surf. Interf. Anal.* **43,** 689–713 (2011).
28. Lang, N. D. & Kohn, W. Theory of metal surfaces: induced surface charge and image potential. *Phys. Rev. B* **7,** 3541–3550 (1973).
29. Liebsch, A. Electronic screening at metal surfaces and the connection with physical phenomena. *Phys. Scr.* **35,** 354 (1987).
30. Wachter, G. *et al.* Electron rescattering at metal nanotips induced by ultrashort laser pulses. *Phys. Rev. B* **86,** 035402 (2012).

Supplementary Information is available in the online version of the paper.

Author Contributions S.N. conceived the material system for this study and performed preparatory experiments. S.N., A.L.C., P.F., E.M., R.E. and R.K. designed and developed the experiment. S.N., R.E. and A.L.C. performed the measurements (with the assistance of E.M., M.J. and E.M.B.). S.N. and R.E. analysed the data. C.L. and S.N. performed the ballistic electron simulations. G.W. and C.L. performed the TDDFT calculations. M.H. and U.K. developed and prepared the XUV multilayer optics. S.N., R.E., C.L., J.B. and R.K. wrote the manuscript with input from the other authors. R.K. and F.K. initiated the project and R.K., F.K. and P.F. supervised the project. All authors discussed the results and conclusions drawn from them.

Author Information Reprints and permissions information is available at www.nature.com/reprints. The authors declare no competing financial interests. Readers are welcome to comment on the online version of the paper. Correspondence and requests for materials should be addressed to S.N. (sneppl@lbl.gov) and R.K. (reinhard.kienberger@tum.de).